# Density modes in spherical $^4$He shells

M. Barranco,[1] E. S. Hernández,[2] R. Mayol,[1] and M. Pi[1]
[1]*Departament d'Estructura i Constituents de la Matèria, Facultad de Física, Universitat de Barcelona, E-08028 Barcelona, Spain*
[2]*Departamento de Física, Facultad de Ciencias Exactas y Naturales, Universidad de Buenos Aires, 1428 Buenos Aires, and Consejo Nacional de Investigaciones Científicas y Técnicas, Argentina*
(Received 9 December 2003; published 7 April 2004)

We compute the density-fluctuation spectrum of spherical $^4\mathrm{He}_N$ shells adsorbed on the outer surface of $C_n$ fullerenes. The excitation spectrum is obtained within the random-phase approximation, with particle-hole elementary excitations and effective interaction extracted from a density-functional description of the shell structure. The presence of one or two solid helium layers adjacent to the adsorbing fullerene is phenomenologically accounted for. We illustrate our results for a selection of numbers of adsorbed atoms on $C_{20}$, $C_{60}$, and $C_{120}$. The hydrodynamical model that has proven successful to describe helium excitations in the bulk and in restricted geometries permits to perform a rather exhaustive analysis of various fluid spherical systems, namely, spheres, cavities, free bubbles, and bound shells of variable size.

DOI: 10.1103/PhysRevB.69.134502 PACS number(s): 67.40.Db, 05.30.Jp, 68.08.Bc, 67.40.Yv

## I. INTRODUCTION

The physics of quantum fluids in restricted geometries is a burgeoning field that has received substantial input during the last decade.[1] Its richness streams mostly from three main sources. One is the adsorption of gases and liquids on substrates of different shapes and degrees of confinement such as planar surfaces, aerogels, carbon nanotubes, and nanotube bundles, giving rise to a variety of wetting phenomena and film growth, which may include dimensionality transitions.[2] The other branches that feed this discipline are the production and analysis of helium clusters,[3,4] and the processes of nucleation and cavitation that lead to the formation of drops and bubbles in the bulk of liquid helium isotopes and their mixtures.[5] The latter two topics involve finite helium systems where the size parameter is the number of atoms, rather than the atom density in one or two dimensions as in e.g., fluid adsorption.

Recently, it has been shown that wetting and cluster physics meet in at least two common grounds. The description of the structure of $^4\mathrm{He}_{N_4}$ and $^3\mathrm{He}_{N_3}+{}^4\mathrm{He}_{N_4}$ clusters formed on planar surfaces made possible the prediction of a new class of single-particle (sp) states for $^3$He atoms added to a deposited $^4\mathrm{He}_{N_4}$ drop,[6] and to a more microscopic interpretation of the transition from nonwetting to wetting of alkalis by fluid $^4$He.[7] Furthermore, anticipating the possibility of confining fullerenes in optical traps and exposing them to a helium atmosphere, an investigation of atom adsorption on spherical substrates has been presented, which also provides a detailed study of the growth of spherical helium shells in the outer adsorbing field of fullerenes as the number of adatoms increases.[8] A similar approach has been applied to study the structure of the free surface in these bound shells.[9] Although advances in the computational applications of microscopic many-body techniques, Such as correlated variational or Monte Carlo methods, bring in the possibility to rely on first-principle calculations to describe complex quantum fluid systems, this is not always the case when nontrivial geometries dominate[6,7] or when fermionic $^3$He is involved.[10] More phenomenological methods based on finite-range density functionals (FRDF's) have proven reliable to anticipate behaviors, or to describe experimental findings, in all the branches enumerated above. In general, FRDF results have been found in agreement with available microscopic calculations within cluster and wetting physics. In particular, recent descriptions of the structure of deposited helium droplets[6,7] and adsorption on spherical substrates[8,9] have been performed in the FRDF frame. Since in the latter case, the FRDF structure and energetics of helium films does agree with exact path-integral Monte Carlo calculations,[8] we may safely rely on the validity of the phenomenological approach and undertake one step forward.

In the present work, we investigate the spectrum of density fluctuations of spherical helium shells adsorbed on $C_n$ fullerenes. The theoretical frame to evaluate this spectrum is the random-phase approximation (RPA) and, as in previous related works,[11–14] the elementary excitations of the helium quasiparticles and the particle-hole (ph) residual interaction are obtained by application of the FRDF method. Given that quantum fluid hydrodynamics has also proven to be a trustworthy instrument to describe capillarity waves and density fluctuations in helium films adsorbed in the interior of cylindrical pores and on planar substrates,[15] we develop the corresponding spectrum for spherical shells on the outer surface of an attracting fullerene. This method enables us to perform a systematic analysis of the excitation spectrum as a function of the number of adsorbed atoms, as well as to elucidate the consequences of suppressing the most tightly bound layers adjacent to the substrate.

This paper is organized as follows. In Sec. II we shortly review the RPA formalism for finite helium systems, and in Sec. III we discuss the FRDF approach here employed and present typical patterns of spherical helium shells and their collective excitations. The hydrodynamic description and calculations are presented in Sec. IV, and this work is summarized in Sec. V.

 

## II. EXCITATIONS OF $^4$He SHELLS ADSORBED ON SPHERICAL SURFACES

We shall apply the RPA formalism, as derived for spherical fermion[16] and boson[11] systems at zero temperature and employed in several applications to doped $^4$He (Refs. 12 and 13) and $^3$He droplets (Ref. 14) In view of existing refined calculations for pure and doped helium systems that employ correlated variational[17] and Monte Carlo[18] techniques (see also Refs. 1 and 4), one may be reassured that the simple RPA method combined with a FRDF description provides the main trends of the density-fluctuation spectrum. In this frame, one searches the poles of the density-density Green's function[19] that solves the RPA integral equation,

$$G^{RPA}(\mathbf{r}_1,\mathbf{r}_2,\omega)=G^0(\mathbf{r}_1,\mathbf{r}_2,\omega)+\int d\mathbf{r}_3\, d\mathbf{r}_4 G^0(\mathbf{r}_1,\mathbf{r}_3,\omega) \times V^{ph}(\mathbf{r}_3,\mathbf{r}_4)G^{RPA}(\mathbf{r}_4,\mathbf{r}_2,\omega). \quad (1)$$

Here $G^0(\mathbf{r}_1,\mathbf{r}_2,\omega)$ is the free ph Green's function and $V^{ph}$ is the residual ph interaction. For $N$ bosons at zero temperature, this reads

$$G^0(\mathbf{r}_1,\mathbf{r}_2,\omega)=N\sum_n \left\{ \frac{\phi_0^*(\mathbf{r}_1)\phi_0(\mathbf{r}_2)\phi_n^*(\mathbf{r}_2)\phi_n(\mathbf{r}_1)}{\hbar\omega-(e_n-e_0)+i\zeta} - \frac{\phi_0^*(\mathbf{r}_2)\phi_0(\mathbf{r}_1)\phi_n^*(\mathbf{r}_1)\phi_n(\mathbf{r}_2)}{\hbar\omega+(e_n-e_0)+i\zeta}\right\}, \quad (2)$$

where $e_n$ and $\phi_n$, respectively, denote the sp energies and wave functions, $\zeta$ is a small energy parameter, $\phi_0(\mathbf{r})$ is the sp wave function of the Bose condensate, and the sum runs over all excited sp states. The RPA transition density $\delta\rho(\mathbf{r})$ induced by a one-body excitation field $V^{ext}(\mathbf{r})$ is

$$\delta\rho(\mathbf{r},\omega)=\int d\mathbf{r}'\, G^{RPA}(\mathbf{r},\mathbf{r}',\omega)V^{ext}(\mathbf{r}') \quad (3)$$

and the dynamical susceptibility or response function $\chi(\omega)$ takes the form

$$\chi(\omega)=\int d\mathbf{r}\delta\rho(\mathbf{r},\omega)V^{ext}(\mathbf{r}). \quad (4)$$

The poles of $\chi(\omega)$ yield the collective excitations of the system stimulated by $V^{ext}$, and the strength function $S(\hbar\omega)=-\mathrm{Im}\chi(\hbar\omega)/\pi$ reads

$$S(\hbar\omega)=\sum_m |\langle m|V^{ext}|0\rangle|^2\delta(\hbar\omega-E_{m0}), \quad (5)$$

where $|0\rangle$ is the RPA ground state (gs), and $|m\rangle$, $E_{m0}$ are RPA excited states and energies, respectively.

Our system of interest is a spherical helium shell adsorbed on the outer surface of a carbon sphere of radius $R$. The substrate field $V_C(r,R)$ experienced by one adatom at distance $r-R$ from the surface is taken to be the angular integral of the Lennard-Jones (LJ) potential between one helium and one carbon atom, assuming a constant areal density of the latter on the sphere.[8] To compute the density fluctuations of the film, we first derive the elementary excitation spectrum $e_n$ of the helium quasiparticles as done in Ref. 8, starting from the FRDF of Ref. 7,

$$E[\rho]=\int d\mathbf{r}\left\{\frac{\hbar^2}{2m}\sum_i^N |\nabla\phi_i(\mathbf{r})|^2+\frac{c'}{2}\rho(\mathbf{r})\,\tilde{\rho}^2(\mathbf{r}) + \frac{c''}{3}\rho(\mathbf{r})\,\tilde{\rho}^3(\mathbf{r})+V_C(r,R)\rho(\mathbf{r}) + \frac{1}{2}\rho(\mathbf{r})\int d\mathbf{r}'\rho(\mathbf{r}')V(|\mathbf{r}-\mathbf{r}'|)\right\}. \quad (6)$$

In this equation, $\tilde{\rho}(\mathbf{r})$ is the coarse-grained density,

$$\tilde{\rho}(\mathbf{r})=\int d\mathbf{r}'\,\rho(\mathbf{r}')\mathcal{W}(|\mathbf{r}-\mathbf{r}'|), \quad (7)$$

where the weighting function $\mathcal{W}(r)$ reads

$$\mathcal{W}(r)=\begin{cases} 3/(4\pi h^3) & \text{if } r\geqslant h \\ 0 & \text{if } r\leqslant h. \end{cases} \quad (8)$$

The finite range interaction consists of a screened LJ potential,

$$V_{LJ}(r)=\begin{cases} 4\varepsilon[(\sigma/r)^{12}-(\sigma/r)^6] & \text{if } r\geqslant h \\ V_0(r/h)^4 & \text{if } r\leqslant h \end{cases} \quad (9)$$

with $\varepsilon=10.22$ K, $\sigma=2.556$ Å, and $h=2.359\,665$ Å. The value of the hard-core radius $h$ has been fixed so that the volume integral of $V_{LJ}$ coincides with the one in Ref. 20. Notice that $V_0$ is the value of the 6-12 potential at $r=h$. The remaining parameters are $c'=-2.411\,86\times10^4$ K Å (Ref. 6) and $c''=1.85850\times10^6$ K Å.[9]

Since at zero temperature all particles belong to the Bose condensate, the particle and kinetic-energy density, respectively, read

$$\rho(\mathbf{r})=\sum_n |\phi_n(\mathbf{r})|^2=N|\phi_0(\mathbf{r})|^2, \quad (10)$$

$$\frac{\hbar^2}{2m}\sum_n |\nabla\phi_n(\mathbf{r})|^2=\frac{\hbar^2}{2m}N|\nabla\phi_0|^2=\frac{\hbar^2}{2m}\frac{1}{4}\frac{(\nabla\rho)^2}{\rho}. \quad (11)$$

The sp wave functions $\phi_n$ and energies $e_n$ are the solutions of the Hartree equation,

$$\left[-\frac{\hbar^2}{2m}\Delta+\frac{\delta U}{\delta\rho}\right]\phi_n=e_n\phi_n \quad (12)$$

obtained by functional differentiation of the total energy, where $U[\rho]$ is the potential energy in Eq. (6), and $\delta U/\delta\rho$ the mean field that includes the substrate potential $V_C(r,R)$. The ph interaction $V^{ph}$ is given by the second functional derivative of the total energy with respect to the particle gs density, i.e.,

$$V^{ph}(\mathbf{r},\mathbf{r}')=\frac{\delta^2 E[\rho]}{\delta\rho(\mathbf{r})\,\delta\rho(\mathbf{r}')}. \tag{13}$$

A straightforward calculation gives

$$V^{ph}(\mathbf{r},\mathbf{r}')=V(|\mathbf{r}-\mathbf{r}'|)+\{c'[\tilde{\rho}(\mathbf{r})+\tilde{\rho}(\mathbf{r}')]+c''[\tilde{\rho}^2(\mathbf{r})+\tilde{\rho}^2(\mathbf{r}')]\}\mathcal{W}(|\mathbf{r}-\mathbf{r}'|)+\int d\mathbf{r}''\,\rho(\mathbf{r}'')[c'+2\,c''\tilde{\rho}(\mathbf{r}'')]\mathcal{W}(|\mathbf{r}-\mathbf{r}''|)\mathcal{W}(|\mathbf{r}''-\mathbf{r}'|). \tag{14}$$

It should be kept in mind that the substrate potential is a one-body field that does not enter the ph interaction explicitly; however, the Hartree equation (12) reveals that this field strongly influences the particle density, thus affecting $V^{ph}$.

As shown in previous works,[11,12] given a multipolar external perturbation $V_l^{ext}(\mathbf{r})=r^l Y_{l0}(\hat{\mathbf{r}})$, one derives RPA equations for the $l$th component of the Green function $G_l^{RPA}(r_1,r_2,\omega)$ in terms of the ph interaction $V_l^{ph}(r_1,r_2)$, defined through the expansions

$$G^{RPA}(\mathbf{r}_1,\mathbf{r}_2,\omega)=\sum_{l,m} G_l^{RPA}(r_1,r_2,\omega)Y_{lm}^*(\hat{\mathbf{r}}_1)Y_{lm}(\hat{\mathbf{r}}_2), \tag{15}$$

$$V^{ph}(\mathbf{r}_1,\mathbf{r}_2)=\sum_{l,m} V_l^{ph}(r_1,r_2)Y_{lm}^*(\hat{\mathbf{r}}_1)Y_{lm}(\hat{\mathbf{r}}_2). \tag{16}$$

The $l$th component of the free ph Green's function is

$$G_l^0(r_1,r_2,\omega)=\frac{N}{4\pi}\sum_n \mathcal{R}_{00}(r_1)\mathcal{R}_{00}(r_2)\times\left\{\frac{1}{\hbar\omega-(e_{nl}-e_0)+i\zeta}-\frac{1}{\hbar\omega+(e_{nl}-e_0)+i\zeta}\right\}\mathcal{R}_{nl}(r_1)\mathcal{R}_{nl}(r_2). \tag{17}$$

Here the sp wave function is defined as $\phi_{nl}(\mathbf{r})=\mathcal{R}_{nl}(r)Y_{lm}(\hat{\mathbf{r}})$, corresponding to a sp energy $e_{nl}$. The summation runs over all the excited Hartree states of multipolarity $l$. The transition density and the response function are then naturally decomposed into multipoles $\delta\rho_l(r,\omega)$, $\chi_l(\omega)$. Consequently, the RPA problem consists of finding the solution of a one-dimensional integral equation for each $l$ (see Refs. 11 and 12 for details).

RPA calculations within the density-functional formalism thus request the previous computation of density profiles and sp spectrum for the selected number of atoms in the external field $V_C(r,R)$. The analysis of the solutions of Eq. (12) for helium adsorbed on the outer surface of carbon fullerenes has been presented in Refs. 8 and 9, where it has been shown that adsorbed helium films grow according to a sequence of layers. For low numbers of helium atoms, the submonolayer peaks at a distance $r_1=3.15$ Å from the sphere surface, which roughly coincides with the location of the centroid $\langle r\rangle=\int_R^\infty dr\,r^2\,\rho(r)$ of the mass distribution, and second layer promotion takes place at an areal density $N/(4\pi\langle r\rangle^2)=0.11$ Å$^{-2}$, as reported in earlier experiments of helium film growth on planar graphite.[21] Similarly, a third layer starts forming at a coverage near 0.2 Å$^{-2}$. Since in planar films, the first (second) layer is solid when the second (third) layer starts forming, we may assume that this structural feature is preserved in the spherical geometry. If we adopt the phase diagram of helium on graphite,[21] a submonolayer transition from fluid to commensurate solid would be expected at a number of atoms around $N_1=0.04\,(4\pi\langle r\rangle^2)$ and monolayer completion—in the shape of an incommensurate solid—should occur at $N_s=0.011\,(4\pi\langle r\rangle^2)$.

Since the RPA formalism described above assumes that all helium atoms are in the liquid phase, it has to be generalized to accommodate the physical situation in which the first helium layers are solid. One possibility is to adopt the treatment by Clements *et al.*;[22] in this case, for a planar geometry the first two planes of helium are modeled by averaging suitable LJ He-graphite potentials, so that only the helium atoms outside these layers are handled explicitly. A similar approach has been proposed by Pricaupenko and Treiner,[23] who substitute the solid layers by Gaussian distributions, conveniently normalized and placed. We adopt here a different prescription to split the total number of He atoms into a solid and a liquid part. According to the previous discussion, we have a criterion to establish, for a given fullerene and a total number $N$ of $^4$He atoms, the amount $N_s$ in the first solid layers, while $N_l=N-N_l$ remain in the liquid shells. The structure of the solid shells is obtained by solving the Hartree equation (12) for $N_s$, which yields a local density $\rho_s(\mathbf{r})$ that remains frozen thereafter.

The structure of the liquid shells is next encountered from the solution, for $N_l$ atoms at density $\rho_l(\mathbf{r})$, of the Hartree equation obtained by functional differentiation of $E[\rho=\rho_s+\rho_l]$ with respect to $\rho_l$, keeping $\rho_s(\mathbf{r})$ fixed as the previously determined function. The ph interaction $V^{ph}$ is then given by Eq. (14) with $\rho=\rho_s+\rho_l$, and $\tilde{\rho}=\tilde{\rho}_s+\tilde{\rho}_l$.

Our way of treating the solid layers, certainly as crude as other previous prescriptions,[22,23] attempts at distinguishing in the system those atoms (in the liquid) that participate in the collective oscillations, from those (in the solid) tightly bound to the substrate, and the substrate itself. It is worth noting that, typically, the oscillation energies of fullerenes are in the range $10^2$–$10^3$ K,[24] well above those of the liquid helium shell.

## III. DENSITY-FUNCTIONAL RESULTS

In this section we illustrate our results for three $C_n$ fullerenes, namely, $n=20$, 60, and 120, their respective radii $R_n$ being 2.05, 3.55, and 5.00 Å. In Fig. 1 we plot the density profiles of a shell containing 25 $^4$He atoms on these fullerenes, which may be regarded as purely fluid particles. For larger numbers of atoms, the presence of one or two solid layers has been removed as indicated. To illustrate this point, in Fig. 2 we plot the density profiles for $N_l+N_s=100$ helium atoms on $C_{60}$, with $N_l=35$ liquid atoms, i.e., those that remain once a previously computed shell with

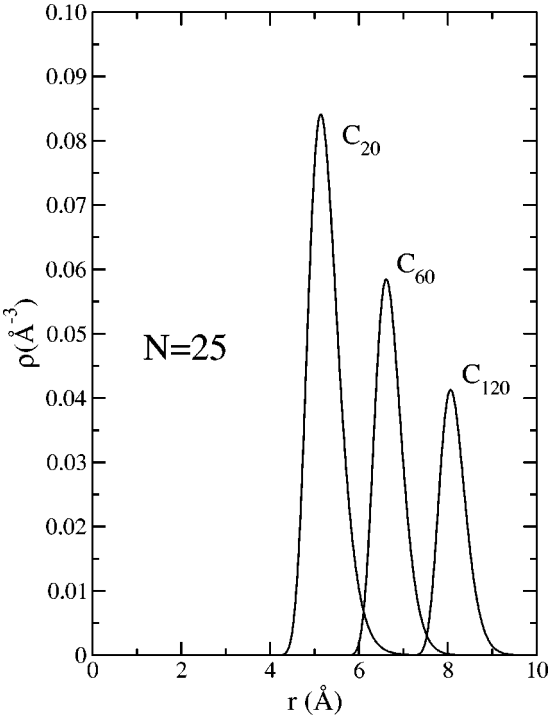


FIG. 1. Atomic densities for $^4He_{25}$ on three different fullerenes $C_n$ with $n=20$, 60, and 120.

$N_s=65$ solid atoms—essentially the integral of the particle density under the first peak, see, i.e., Ref. 8—has been subtracted. As anticipated in Sec. II, although $N_s$ atoms are inert in the latest computation, their density $\rho_s(r)$, displayed as a peak in dashed lines in Fig. 2, enters the mean field experienced by the $N_l$ particles; consequently, the solid density does influence the density profile and residual ph interaction of the active atoms. In Fig. 3, a similar plot is displayed for the case of 500 atoms on $C_{120}$; in this case, two solid layers are present with total $N_s=155$ particles. As indicated in the preceding section, we shall consider that for a given number of helium atoms adsorbed on the carbon sphere, only $N_l=N-N_s$ atoms participate in ph transitions when excited by an external, long wavelength multipole field.

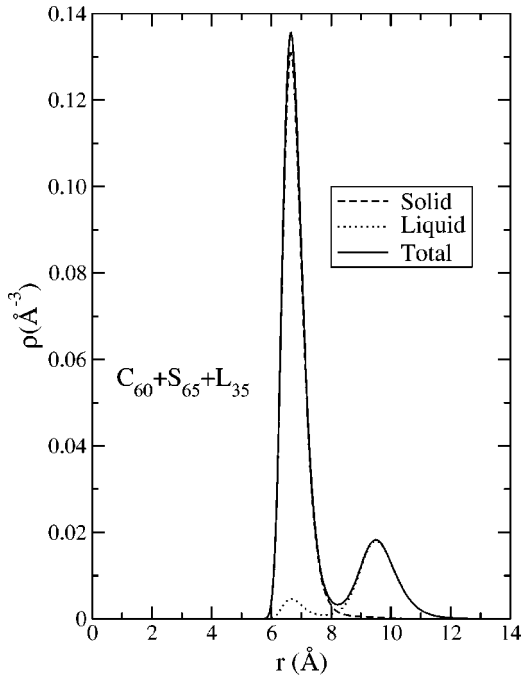


FIG. 2. Atomic densities for $^4He_{100}$ on $C_{60}$. Dotted line, liquid density (35 atoms); dashed line, solid density (65 atoms), solid line, total density (100 atoms).

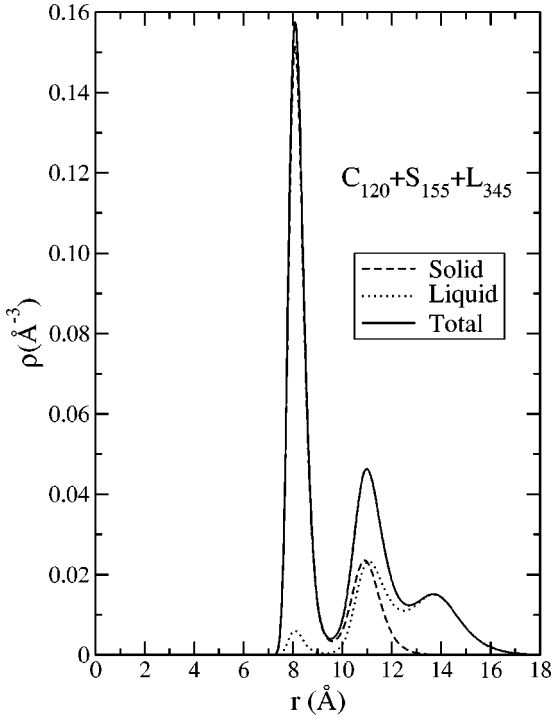


FIG. 3. Atomic densities for $^4He_{500}$ on $C_{120}$. Dotted line, liquid density (345 atoms); dashed line, solid density (155 atoms), solid line, total density (500 atoms).

We have performed specific calculations for external fields $V_0^{ext}=r^2Y_{00}$ for $l=0$, and $V_l^{ext}(\mathbf{r})=r^lY_{l0}(\hat{\mathbf{r}})$ for $l=1$ to 3. It should be noted that there is a nontrivial dipole mode that represents the displacement of the liquid shell against the solid layers plus the fullerene as a whole. This dipole mode is obviously absent in pure helium droplets.

Our results for the multipolar strengths $S_l(\omega)$, for $l=0$ to 3, are displayed in Figs. 4–6, which respectively correspond to $N=N_l=25$ on $C_{20}$ (cf. Fig. 1); $N_l=35$, $N_s=65$ on $C_{60}$ (cf. Fig. 2); and $N_l=345$, $N_s=155$ on $C_{120}$ (cf. Fig. 3). In these figures, the strengths have been normalized so that, for each $l$, the maximum peak height is unity.

It can be seen that for $l>0$ the strength is concentrated in a single collective peak. This peak exhausts most of the energy-weighted $m_1$ sum rule[12]

$$m_1=\sum_m E_{m0}|\langle m|V^{ext}|0\rangle|^2$$

$$=\int_0^\infty E\,S(E)\,dE=\frac{\hbar^2}{2m}\int d\mathbf{r}\,\rho(\mathbf{r})(\boldsymbol{\nabla}V^{ext})^2, \quad (18)$$

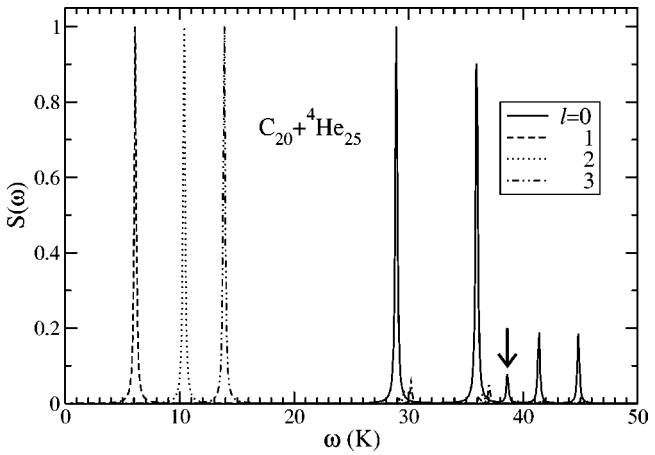


FIG. 4. Strength functions for $l=0$ to 3 for $C_{20}+{}^4He_{25}$. The arrow indicates the atom emission threshold. Strength functions have been normalized so that, for each *l*, the maximum peak height is unity.

which, for $l=1$, becomes the Thomas-Reiche-Kuhn sum rule

$$m_1(l=1)=\frac{\hbar^2}{2m}\frac{3}{4\pi}N. \tag{19}$$

It is also worth noting that these narrow resonances are at energies below the atom emission threshold, which for $C_{20}+{}^4He_{25}$ is indicated by an arrow in Fig. 4. For $C_{60}+{}^4He_{100}$ it lies at 12.9 K, and for $C_{120}+{}^4He_{500}$, at 7.5 K.

## IV. CAPILLARY AND DENSITY WAVES IN THE HYDRODYNAMIC APPROXIMATION

Capillary waves in spherical fluid drops and cavities are analyzed in textbooks[25,26] and the specific derivation of hydrodynamic density waves of helium films in the interior of cylindrical pores has been presented in Ref. 15. Here we model our helium system as a shell of density $\rho_0$ surrounding a spherical substrate of radius $R$ and extending up to a sharp

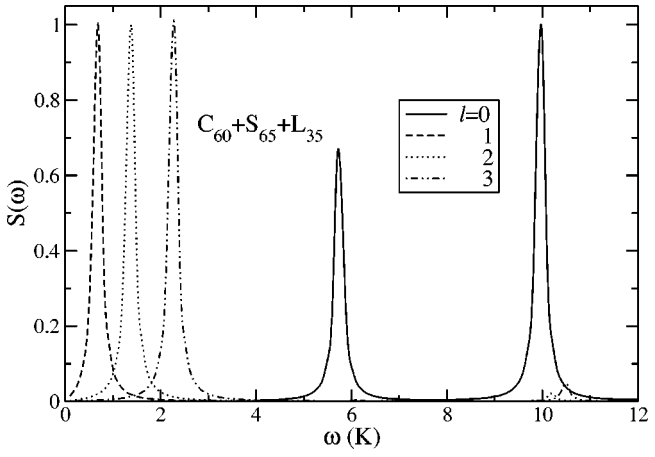


FIG. 5. Strength functions for $l=0$ to 3 for $C_{60}+{}^4He_{100}$. They have been normalized so that, for each *l*, the maximum peak height is unity.

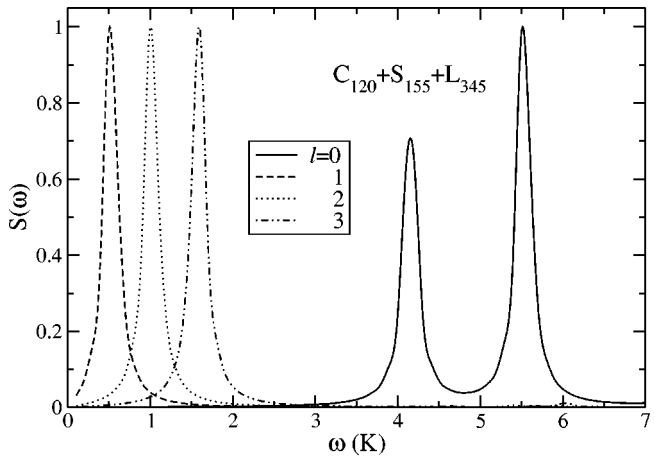


FIG. 6. Strength functions for $l=0$ to 3 for $C_{120}+{}^4He_{500}$. They have been normalized so that, for each *l*, the maximum peak height is unity.

radius $a$. Our simple model also assumes that the substrate potential is piecewise constant, with nonvanishing finite derivative $U'(a)\equiv V'(a,R)$. Figure 7 contains size parameters of interest for the growth of helium films on $C_{60}$, where $\langle r\rangle$ and $\delta r$ are, respectively, the centroid and the dispersion of the density profile for the given $N$ as discussed in Ref. 8, and $a$ is the hydrodynamic radius defined by

$$N=\frac{4\pi}{3}(a^3-R^3)\,\rho_0 \tag{20}$$

with $R\equiv R_{60}=3.55$ Å.

To derive the modes one starts from the linearized continuity and momentum conservation equations for superfluid flow,

$$\frac{\partial\rho}{\partial t}=-\rho_0\,\nabla\cdot\mathbf{v}_s, \tag{21}$$

$$m\,\rho_0\frac{\partial\mathbf{v}_s}{\partial t}=-\nabla P-\rho_0\,\nabla U \tag{22}$$

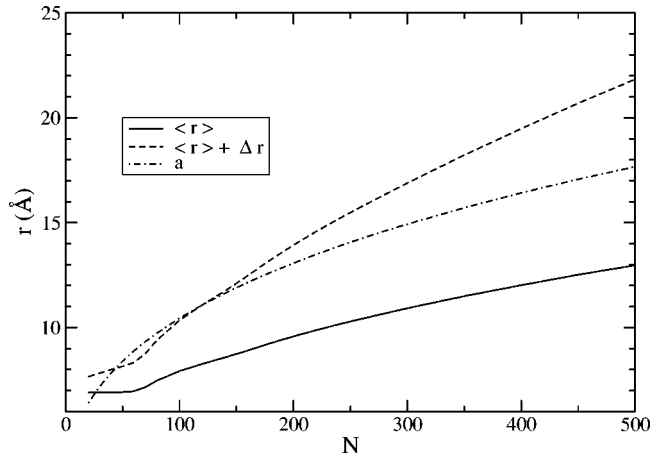


FIG. 7. Mean radius, mean radius plus dispersion, and hydrodynamic radius $a$ as functions of the number of atoms.

with $\rho_0$ the bulk density and $U(r)$ the spherically symmetric external potential on a single helium atom of mass $m$. We establish the following

(a) The pressure at any free surface is the Laplace pressure of a deformable sphere with undistorted radius $a$,

$$P=\sigma\left(\frac{1}{R_1}+\frac{1}{R_2}\right)=\sigma K_0-\frac{1}{a^2}(2+\nabla_\Omega^2)\,\eta, \tag{23}$$

where $\sigma$ is the liquid surface tension, $\eta$ is the displacement of the surface, $K_0=1/a$ is the spherical curvature, and $\nabla_\Omega^2$ is the angular part of the Laplacian operator.

(b) The superfluid flow condition, $\mathbf{v}_s=\boldsymbol{\nabla}\varphi(\mathbf{r})$, where $\varphi(\mathbf{r})$ is the velocity potential.

(c) Boundary conditions (bc's): on a spherical wall located at position $R$, $\mathbf{v}_s\cdot\hat{n}_w=0$; on a spherical free surface at position $a$, $\mathbf{v}_s\cdot\hat{n}_s=\partial\eta/\partial t$, with $\hat{n}_w$, $\hat{n}_s$ the unit vector perpendicular to the corresponding surface, one reaches the system for the wave equation with the given bc's,

$$\nabla^2\varphi+\frac{\omega^2}{c_s^2}\varphi=0, \tag{24}$$

$$\mathbf{v}_s\cdot\hat{n}_w=0, \tag{25}$$

$$g_l(a)\left.\frac{d\varphi_l}{dr}\right|_a=\omega^2\,\varphi_l(a). \tag{26}$$

Here $c_s$ is the sound velocity in bulk helium. In Eq. (26) it has been already assumed that the velocity potential is of the form $\varphi(\mathbf{r})=\varphi_l(r)\,Y_{lm}(\hat{\mathbf{r}})$. Moreover, we have introduced the effective gravity

$$g_l(a)=g(a)+g_l^0(a)=\frac{1}{m}\boldsymbol{\nabla}U\cdot\hat{n}_s+\frac{\sigma}{\rho_0 m a^2}(l-1)\,(l-2) \tag{27}$$

that adds the "substrate gravity" $g=U'(a)/m$ to the "capillarity gravity" $g_l^0(a)$. We also note that in Ref. 15 an equivalent system has been solved for fully and partially filled cylindrical pores and for planar films.

Capillary waves of incompressible fluid systems are obtained solving Laplace's equation $\boldsymbol{\nabla}\varphi_l(r)=0$ for the velocity potential with the corresponding bc's. If propagation of density fluctuations is allowed—i.e., if the fluid is compressible—one seeks perturbations $\delta\rho(r)$ proportional to the solution $\varphi(r)$ of the wave equation, together with a dispersion relation $\omega=c_s\,q$. Expansion of the solutions up to second order in $q^2$ leads then to the eigenfrequencies $\omega_l(a)$, for $l>0$, in the long wavelength limit. Note that the oscillation modes of an incompressible sphere (capillary waves), which correspond to the solutions of Laplace's equation with bc (26), are derived in Refs. 25 and 26 assuming a velocity potential of the form $\varphi_l(r)=r^l(l>0)$. The frequencies read

$$[\omega_l^0(a)]^2=\frac{g_l^0(a)\,l}{a}. \tag{28}$$

For a helium sphere with $N$ atoms, this is complemented by the relation $\rho_0=3N/(4\pi a^3)$. No monopole modes can be supported by an incompressible sphere.

In this work, we first solve for the capillary waves of an incompressible helium shell adsorbed on a sphere, with velocity potential

$$\varphi_l(r)=r^l+\frac{l}{l+1}\frac{R^{2l+1}}{r^{l+1}} \tag{29}$$

$(l>0)$. This form is chosen to satisfy the bc at the wall, while the one on the free surface gives the dispersion relation

$$\omega_{l_{inc}}^2=\frac{g_l(a)\,l\,(l+1)}{a}\frac{1-u_l}{l+1+l\,u_l}. \tag{30}$$

Here we have introduced the dimensionless ratio $u_l\equiv(R/a)^{2l+1}$. Expression (30) coincides with the modes (28) of an incompressible sphere when $R=u_l=0$ and $g_l(a)=g_l^0(a)$. For the compressible shell, the density fluctuation $\delta\rho(r)$ is proportional to the velocity potential, taken as

$$\varphi_l(r)=j_l(qr)-\frac{j_l'(qR)}{n_l'(qR)}n_l(qr) \tag{31}$$

with $j_l(z)$,$n_l(z)$ the regular and irregular spherical Bessel functions.[27] Expansion of these functions in the bc (26) up to their second-order terms gives the eigenfrequencies for $l>0$ in the long wavelength limit

$$\omega_l^2=\frac{\omega_{l_{inc}}^2}{1+\dfrac{\omega_{l_{inc}}^2 a^2}{2c_s^2(1-u_l)}\left[\dfrac{l-1}{(l+1)(2l-1)}(u_l-u_0^2)+\dfrac{(l+2)}{l(2l+3)}(1-u_0^2u_l)\right]} \tag{32}$$

with $u_0\equiv u_{l=0}$.

The monopole frequencies of the compressible film are obtained after expanding Eq. (26) so as to keep terms of order $q^4$. In this way we get

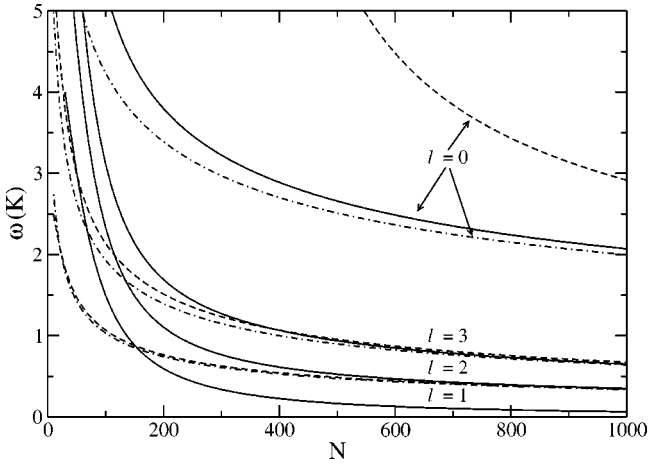


FIG. 8. The oscillation modes of compressible helium shells adsorbed on $C_{60}$ (full lines) as functions of the number of particles, for $l=0$ to 3. Dashed and dot-dashed lines, respectively, correspond to the coherent mode of free shells and to spheres of the same number of atoms (see the Appendix for details). Both the inner surface radius of the free shell and the substrate radius for the bound system are taken as radius $R_{60}$.

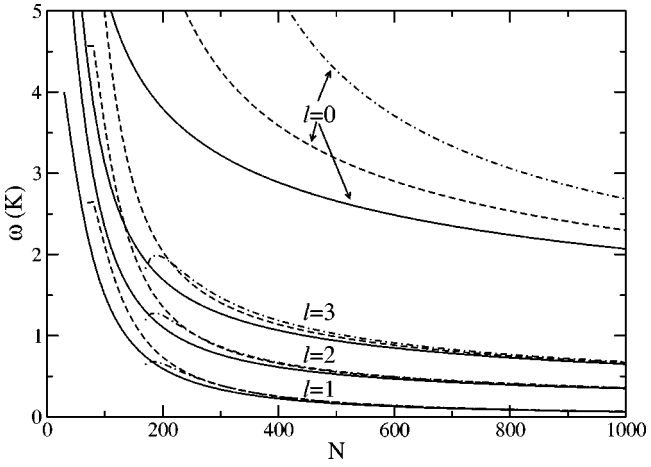


FIG. 9. Spectrum of density waves of helium shells adsorbed on $C_{60}$ as a function of atom number for $N$ fluid atoms (full lines), $N-65$ fluid atoms on a sphere of radius $R+3.15$ Å, and for $N-155$ fluid atoms on a sphere of radius $R+6.05$ Å.

$$\omega_0^2 = 6\frac{c_s^2}{a^2}\frac{1+\dfrac{g_0(a)\,a}{3\,c_s^2}(1-u_0^3)}{1-3\,u_0^2+2\,u_0^3+\dfrac{g_0(a)\,a}{5\,c_s^2}(1-5\,u_0^2+5\,u_0^3-u_0^5)}. \tag{33}$$

We have computed the dispersion relations (30), (32), and (33) for shells adsorbed on $C_n$ fullerenes; for reference, we have also calculated the corresponding eigenfrequencies for capillary and density waves of spheres and free shells, whose expressions are collected in the Appendix. Typical results are displayed in Fig. 8 where we plot the spectrum of density waves of shells adsorbed on $C_{60}$ as functions of the number of atoms, together with those of spheres and free shells, for $l=0$ to 3. The general features of these hydrodynamic modes are the following. First, we encounter that in all cases, at low numbers of fluid atoms the eigenenergies of compressible systems are lower than those of the incompressible ones. This difference disappears for a few hundreds of particles. Moreover, for sufficiently large number of fluid atoms, the common compressible and incompressible eigenenergies collapse onto those of a sphere with the same particle number. Finally, it can be seen that at low particle number, a shell bound to $C_{60}$ is ''stiffer'' than a free shell—i.e., the oscillation energies are higher, revealing the presence of the substrate gravity in addition to the capillarity pressure. This effect disappears for sufficiently large shells, roughly above 500 atoms.

In Fig. 9 we illustrate the influence of subtracting solid layers. For $l=0$ to 3, full lines denote the spectrum of $N_l=N$ atoms adsorbed on $C_{60}$, dashed lines correspond to subtracting a first solid layer with $N_s=65$, and dot-dashed lines correspond to removing two solid layers with total $N_s=155$. In the latter two cases, the sphere radius has been moved to the location of the first and second peak in the mass distribution of the inert particles, respectively. We appreciate that while for $l>0$ multipolarities the modes are not influenced by the removal of solid atoms for, say, $N$ above 400–500, this is not the case for the breathing excitations. It is worth noting, moreover, that the eigenfrequencies in Fig. 9 are in good quantitative agreement—however, slightly smaller—with the RPA results illustrated in Sec. III. This fact permits one to circumvent computationally more demanding calculations, like the RPA+FRDF approach, in order to examine the effects of the inert layers on the density-fluctuation spectrum.

## V. SUMMARY

In this work we have presented a RPA calculation of the density-density response of spherical helium shells adsorbed on carbon fullerenes, for several numbers of helium adatoms. The elementary sp excitations are taken as those in the mean field derived from a FRDF previously employed in a variety of applications to helium systems. This procedure is in the spirit of earlier studies of the spectrum of density fluctuations in doped helium droplets[12–14] and the results are robust and consistent with the expectations for this kind of systems. For the smaller particle numbers here reported, the spectrum is characterized by large fragmentation of the monopole strength, with main peaks lying at energies of order 10 K, and by comparatively smaller eigenenergies for higher multipolarities. Due to the peculiar configuration with a sizable spherical cavity in the fluid, originated in the presence of the fullerene, which shifts the location of the main peak in the mass distribution to around 6 Å, a nontrivial dipole oscillation appears at energies around 1 K. For all multipolarities, the eigenenergies are seen to decrease as the number of atoms increases, while for a given number of atoms, they grow with increasing $l>0$.

For systems sufficient large so as to admit one or more layers adjacent to the adsorbing sphere, we have proposed a method to suppress these layers, which should be solid on a

purely planar graphite substrate. Our approach is slightly different from similar ones employed by other authors[22,23] and pursues the same purpose, namely, to separate inert atoms from those expected to participate in density fluctuations. The hydrodynamic description of these modes seems to point out that the effect of the presence of inert layers becomes irrelevant for particle numbers above a few hundreds of atoms.

We have developed a simple hydrodynamic model for spherical fluid shells on a substrate, which disregards the shell structure and only involves bulk parameters such as helium saturation density and surface tension, and the value of the substrate attractive force on the free surface. The eigenfrequencies can be derived analytically, both for capillary waves of an incompressible helium fluid and for density fluctuations of a compressible system. The results can be displayed as functions of atom number and it is clearly seen that the eigenenergies of these modes vanish monotonically with increasing $N$, keeping the ordering sequence encountered in the RPA calculations. A comparison of spectra of incompressible and compressible spheres, free shells, and shells bound to a substrate shows that geometry effects such as the presence of a solid sphere, as well as the distinction between compressible and incompressible systems, is minute above a few hundred particles.

## ACKNOWLEDGMENTS

This work has been partially supported by grants PID 02391 from Consejo Nacional de Investigaciones Científicas y Técnicas, EX 103 from Universidad de Buenos Aires, and PICT 03-08450 from Agencia Nacional de Promoción Científica y Tecnológica, Argentina; BFM2002-01868 from DGI, Spain, and 2001SGR-00064 from Generalitat of Catalonia.

## APPENDIX

In the spherical geometry, we may consider four mass distributions at bulk density $\rho_0$ corresponding to (a) $N$ atoms on a sphere of radius $a$; (b) a cavity of radius $R$ in the bulk liquid; (c) $N$ atoms in a free shell (''thick'' bubble) between inner and outer radii $R$ and $a$, and (d) $N$ atoms in a shell bound to a substrate of radius $R$ extending up to an outer radius $a$. We list the results below for capillary and density waves, which respectively, correspond to the solutions of Laplace's equation for the case of the incompressible fluid, and to those of the wave equation for the compressible system.

(I) *Capillary waves*. The radial velocity potential chosen as $\varphi_l(r)=A_l r^l+B_l r^{-l-1}$ and the spectrum $\omega_l^2$ for the various incompressible systems of interest are the following.

(1) Incompressible sphere, radius $a$: $A_l=1$, $B_l=0$, and

$$[\omega_l^0(a)]^2=\frac{g_l^0(a)\,l}{a}. \tag{A1}$$

(2) Cavity, radius $R$: $A_l=0$, $B_l=1$, and

$$[\omega_l^0(R)]^2=g_l^0(R)\,\frac{l+1}{R}. \tag{A2}$$

(3) Thick bubble, radii $R<a$: $A_l=1$, and

$$B_l=a^{2l+1}\frac{[\omega_l^0(a)]^2-\omega_l^2}{\omega_l^2+\frac{l+1}{l}[\omega_l^0(a)]^2}=R^{2l+1}\frac{\omega_l^2+[\omega_l^0(R)]^2\frac{l}{l+1}}{[\omega_l^0(R)]^2-\omega_l^2}. \tag{A3}$$

The spectrum exhibits two branches, corresponding to a coherent, low-frequency mode, with the two spherical boundaries oscillating in phase—i.e., the mode to be compared with the density fluctuations of the other systems—and to an incoherent, high-frequency one for the out-of-phase oscillation. These modes are the solutions of the quartic equation $c_4^0\,\omega_l^4+c_2^0\,\omega_l^2+c_0^0=0$ with coefficients

$$c_4^0=1-u_l, \tag{A4}$$

$$c_2^0=-\left\{[\omega_l^0(a)]^2\left(1+\frac{l+1}{l}u_l\right)+[\omega_l^0(R)]^2\left(1+\frac{l}{l+1}u_l\right)\right\}, \tag{A5}$$

$$c_0^0=[\omega_l^0(a)]^2[\omega_l^0(R)]^2\,(1-u_l). \tag{A6}$$

(4) Bound shell, radii $R<a$: $A_l=1$, $B_l=l/(l+1)\,R^{2l+1}$, and

$$[\omega_{l_{inc}}]^2=\frac{g_l(a)\,l\,(l+1)}{a}\,\frac{1-u_l}{l+1+l\,u_l}. \tag{A7}$$

(II) *Density waves*. The density fluctuation is of the form $\delta\rho_l(r)=A_l\,j_l(qr)+B_l\,n_l(qr)$ and the spectra $\omega_l^2$ for $l>0$ are the following.

(1) Sphere, radius $a$: $A_l=1$, $B_l=0$, and

$$[\omega_l(a)]^2=\frac{[\omega_l^0(a)]^2}{1+[\omega_l^0(a)]^2\frac{(l+2)\,a^2}{2\,l\,(2l+3)\,c_s^2}}. \tag{A8}$$

(2) Cavity, radius $R$: $A_l=0$, $B_l=1$, and

$$[\omega_l(R)]^2=\frac{[\omega_l^0(R)]^2}{1-[\omega_l^0(R)]^2\frac{(l-1)\,R^2}{2\,(l+1)\,(2l-1)\,c_s^2}}. \tag{A9}$$

(3) Thick bubble, radii $R<a$: $A_l=1$ and

$$B_l=\frac{g_l^0(a)\,j_l'(qa)-\omega_l^2\,j_l(qa)}{\omega_l^2\,n_l(qa)-g_l^0(a)\,n_l'(qa)}$$

$$=-\frac{g_l^0(R)\,j_l'(qR)+\omega_l^2\,j_l(qR)}{\omega_l^2\,n_l(qR)+g_l^0(R)\,n_l'(qR)}, \tag{A10}$$

where $f'(b)=df(r)/dr|_{r=b}$. After expansion of the spherical Bessel functions, the secular equation for the modes becomes the quartic $c_4\,\omega_l^4+c_2\,\omega_l^2+c_0=0$ with coefficients

$$c_4=c_4^0-\frac{a^2}{2c_s^2}\left\{[\omega_l^0(a)]^2\left[\frac{1}{2l-1}\left(u_0^2+\frac{l-1}{l}u_l\right)-\frac{1}{2l+3}\left(\frac{l+2}{l}+\frac{l+1}{l}u_0^2\,u_l\right)\right]+[\omega_l^0(R)]^2\left[\frac{1}{2l-1}\left(\frac{l}{l+1}u_l+\frac{l-1}{l+1}u_0^2\right)-\frac{1}{2l+3}\left(\frac{l+2}{l+1}u_0^2\,u_l+1\right)\right]\right\}, \tag{A11}$$

$$c_2=c_2^0+\frac{[\omega_l^0(a)]^2[\omega_l^0(R)]^2a^2}{2c_s^2}\left[\frac{l-1}{(l+1)(2l-1)}(u_l-u_0^2)+\frac{l+2}{l(2l+3)}(1-u_0^2u_l)\right], \tag{A12}$$

$$c_0=c_0^0. \tag{A13}$$

(4) Bound shell, radii $R<a$: $A_l=1$, $B_l=-j_l'(qR)/n_l'(qR)$, and upon expansion of the spherical Bessel functions,

$$[\omega_l]^2=\frac{g_l(a)\,l\,(l+1)}{a}\,\frac{1-u_l}{l+1+l\,u_l+\alpha\dfrac{g_l(a)\,a}{2\,c_s^2}} \tag{A14}$$

with

$$\alpha=\frac{l(l+1)}{2l-1}(u_0^2-u_l)+\frac{(l+1)(l+2)}{2l+3}(1-u_0^2u_l). \tag{A15}$$

The monopole modes request one more term in the expansion. The results are the following.

(1) Compressible sphere:

$$\omega_0^2=\frac{6c_s^2}{a^2}\,\frac{1+\dfrac{g_0^0(a)\,a}{3c_s^2}}{1+\dfrac{g_0^0(a)\,a}{5c_s^2}}. \tag{A16}$$

(2) Compressible cavity:

$$\omega_0^2=\frac{g_0^0(R)}{R}\,\frac{1}{1-\dfrac{g_0^0(R)\,R}{2c_s^2}}. \tag{A17}$$

(3) Compressible thick bubble:

$$\omega_0^2=\frac{g_0^0(a)\,g_0^0(R)\,\dfrac{1-u_0^3}{3c_s^2\,u_0}+\dfrac{g_0^0(a)}{a}u_0+\dfrac{g_0^0(R)}{R}}{1-u_0+\dfrac{g_0^0(a)\,a}{c_s^2}\left(\dfrac{1}{3}-\dfrac{u_0}{2}+\dfrac{u_0^3}{6}\right)+\dfrac{g_0^0(R)\,a}{u_0c_s^2}\left(\dfrac{u_0^3}{3}+\dfrac{1}{6}-\dfrac{u_0^2}{2}\right)}. \tag{A18}$$

(4) Compressible bound shell:

$$\omega_0^2=6\,\frac{c_s^2}{a^2}\,\frac{1+\dfrac{g_0(a)\,a}{3\,c_s^2}(1-u_0^3)}{1-3\,u_0^2+2\,u_0^3+\dfrac{g_0(a)\,a}{5\,c_s^2}(1-5\,u_0^2+5\,u_0^3-u_0^5)}. \tag{A19}$$


[1] *Microscopic Approaches to Quantum Liquids in Confined Geometries*, edited by E. Krotscheck and J. Navarro (World Scientific, Singapore, 2002).

[2] M.M. Calbi, M.W. Cole, S.M. Gatica, M.J. Bojan, and G. Stan, Rev. Mod. Phys. **73**, 857 (2001); M.M. Calbi and M.W. Cole, Phys. Rev. B **66**, 115413 (2002); S.M. Gatica, M.M. Calbi, and M.W. Cole, J. Low Temp. Phys. **133**, 399 (2003).

[3] J.P. Toennies and A.F. Vilesov, Annu. Rev. Phys. Chem. **49**, 1 (1998).

[4] K.B. Whaley, Adv. Mol. Vib. Collision Dyn. **3**, 397 (1998); *Helium Nanodroplets: A Novel Medium for Chemistry and Physics*, special issue of J. Chem. Phys **115**, 10065 (2001).

[5] S. Balibar and H.J. Maris, Phys. Today **53** (2), 29 (2000); M. Barranco, M. Guilleumas, M. Pi, and D. M. Jezek, in *Microscopic Approaches to Quantum Liquids in Confined Geometries* (Ref. 1), p. 319; S. Balibar, J. Low Temp. Phys. **129**, 363 (2002).

[6] R. Mayol, M. Barranco, E.S. Hernández, M. Pi, and M. Guilleumas, Phys. Rev. Lett. **90**, 185301 (2003).

[7] M. Barranco, M. Guilleumas, E.S. Hernández, R. Mayol, M. Pi, and L. Szybisz, Phys. Rev. B **68**, 024515 (2003).

[8] E.S. Hernández, M.W. Cole, and M. Boninsegni, Phys. Rev. B **68**, 125418 (2003).
[9] L. Szybisz and I. Urrutia, J. Low Temp. Phys. **134**, 1079 (2004).
[10] E. S. Hernández and J. Navarro, in *Microscopic Approaches to Quantum Liquids in Confined Geometries* (Ref. 1), p. 147.
[11] M. Casas and S. Stringari, J. Low Temp. Phys. **79**, 135 (1990).
[12] M. Barranco and E.S. Hernández, Phys. Rev. B **49**, 12 078 (1994).
[13] S.M. Gatica, E.S. Hernández, and M. Barranco, J. Chem. Phys. **107**, 927 (1997).
[14] F. Garcias, Ll. Serra, M. Casas, and M. Barranco, J. Chem. Phys. **108**, 9102 (2001).
[15] W.F. Saam and M.W. Cole, Phys. Rev. B **11**, 1086 (1975).
[16] G.F. Bertsch and S.F. Tsai, Phys. Rep. **18**, 126 (1975).
[17] S.A. Chin and E. Krotscheck, Phys. Rev. B **45**, 852 (1992); **52**, 10 405 (1995).
[18] M. McMahon, R.N. Barnett, and K.B. Whaley, J. Chem. Phys. **104**, 5080 (1995).
[19] A. L. Fetter and J. D. Walecka, *Quantum Theory of Many-Particle Systems* (McGraw-Hill, New York, 1971).
[20] F. Dalfovo, A. Lastri, L. Pricaupenko, S. Stringari, and J. Treiner, Phys. Rev. B **52**, 1193 (1995).
[21] D.S. Greywall, Phys. Rev. B **47**, 309 (1993).
[22] B.E. Clements, J.L. Epstein, E. Krotscheck, and M. Saarela, Phys. Rev. B **48**, 7450 (1993)
[23] L. Pricaupenko and J. Treiner, J. Low Temp. Phys. **94**, 19 (1994).
[24] D.P. Clougherty and J.P. Gorman, Chem. Phys. Lett. **251**, 353 (1996).
[25] L. D. Landau and E. M. Lifshitz, *Fluid Mechanics* (Pergamon, Oxford 1959).
[26] H. Lamb, *Hydrodynamics* (Dover, New York, 1993).
[27] M. Abramowitz and I. Stegun, *Handbook of Mathematical Functions* (Dover, New York, 1972).